

On Noise Injection in Generative Adversarial Networks

Ruili Feng

University of Science and Technology of China.
ruilifengustc@gmail.com

Deli Zhao

Xiaomi AI Lab.
zhaodeli@gmail.com

Zhengjun Zha

University of Science and Technology of China.
zhazj@ustc.edu.cn

Abstract

Noise injection has been proved to be one of the key technique advances in generating high-fidelity images. Despite its successful usage in GANs, the mechanism of its validity is still unclear. In this paper, we propose a geometric framework to theoretically analyze the role of noise injection in GANs. Based on Riemannian geometry, we successfully model the noise injection framework as fuzzy equivalence on the geodesic normal coordinates. Guided by our theories, we find that the existing method is incomplete and a new strategy for noise injection is devised. Experiments on image generation and GAN inversion demonstrate the superiority of our method.

1 Introduction

Noise injection has attracted more and more attention in the community of generative adversarial networks (GANs) Goodfellow *et al.* (2014). Extensive research works show that it help generate images of high fidelity and variety Karras *et al.* (2019b); Brock *et al.* (2018), stabilize the training procedure Arjovsky & Bottou (2017); Jenni & Favaro (2019), and enhance the robustness of neural networks Srivastava *et al.* (2014); Baskin *et al.* (2018); He *et al.* (2019). Traditional GANs take in randomness only from input latent codes and the GAN frameworks with noise injection seek to inject extra noise directly to intermediate feature spaces of the network, as illustrated in Figure 1. It is interesting to point out that this modification of the generator coincides with the gene expression process, where information from a gene is used in the synthesis of a functional gene product (like proteins). It is well known that genotypes along with environmental factors together determine what the phenotypes will be Via & Lande (1985); Romagosa & Fox (1993); Westcott (1986). From a cognitive aspect, twins share the same genes yet admit subtle differences in appearance. So the gene expression could be modeled as a random output network, where genes control the mean and variance of observable traits, while the environment injects the randomness Denis *et al.* (1997); van Eeuwijk (1996); Bustos-Korts *et al.* (2016). These designs allows genes, with relatively simple structures, to express highly complicated, fine, diverse biological phenotypes. If compared input latents in GANs to genes, then random noise injection plays the role of environmental influences. This bionic principle contributes to the bio-inspired motivation of noise injection, as real world data also contain subtle and abundant details, e.g. textures, wrinkles, and patterns of surroundings, thus posing a challenge for the relatively low-dimensional latents to fit. In practice, extensive experiments in StyleGAN Karras *et al.* (2019b) and BigGAN Brock *et al.* (2018) also confirm its validity.

In this work, we propose a theoretic framework to explain and improve the effectiveness of noise injection. Our framework is motivated from a geometric perspective yet also combined with the

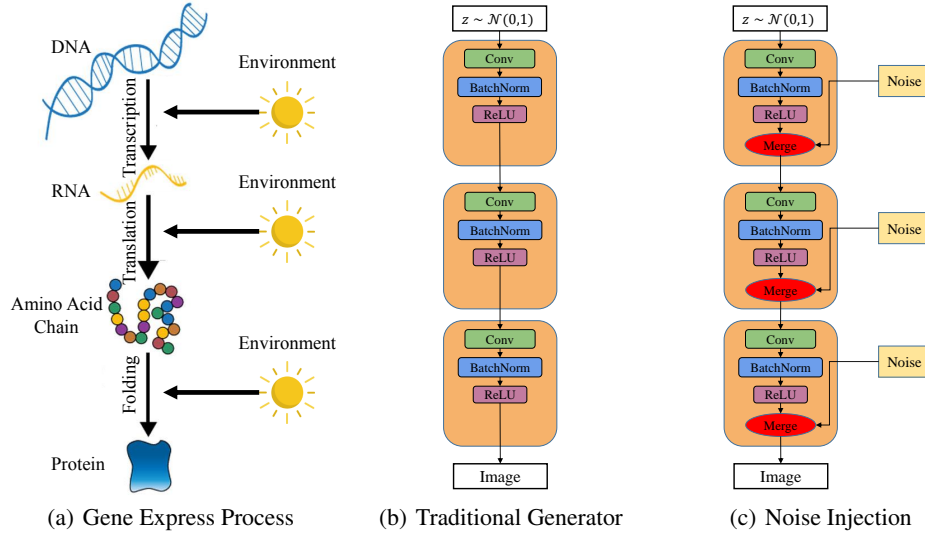


Figure 1: Comparison of gene express process, traditional GAN architecture, and GAN with noise injection.

results of optimal transportation problem in GANs Lei *et al.* (2019b,a). Our contributions are as follows:

- We show that the existing GAN architectures, including the Wasserstein GANs Arjovsky *et al.* (2017), may suffer from adversarial dimension trap, which severely penalizes the property of generator;
- Based on our theory, we try to explain the properties that noise injection are applied in the related literatures;
- Based on our theory, we find a more proper form for noise injection in GANs, which can overcome the adversarial dimension trap, and experiments on the state-of-the-art GAN architecture, StyleGAN2 Karras *et al.* (2019a), demonstrate the superiority of our new method compared with original noise injection used in StyleGAN2.

To the best of our knowledge, this is the first work that theoretically draws the geometric picture of noise injection in GANs.

2 Related Works

The main drawbacks of GANs are unstable training and mode collapse. Arjovsky *et al.* Arjovsky & Bottou (2017) theoretically analyze that noise injection directly to the image space can help smooth the distribution so as to stabilize the training procedure. The authors of Distribution-Filtering GAN (DFGAN) Jenni & Favaro (2019) then put this idea into practice and prove that this technique will not influence the global optimality of the real data distribution. However, as the authors pointed out in Arjovsky & Bottou (2017), this method depends on the amount of noise, and the Jensen-Shannon divergence is not an intrinsic measure of synthesis and data distributions. Actually, our method of noise injection is essentially different from these ones. Besides, they do not provide a theoretical vision of the interactions between injected noises and the features.

BigGAN Brock *et al.* (2018) splits input latents into one chunk per layer as injected noise and project each chunk to the gains and biases of batch normalization in each layer. They claim that this design allows direct influence on features at different resolutions and levels of hierarchy. StyleGAN Karras *et al.* (2019b) and StyleGAN2 Karras *et al.* (2019a) adopt a slightly different view, where noise injection is introduced to enhance randomness for multi-scale stochastic variations. Different from the settings in BigGAN, they inject extra noise independent of the latent inputs into different layers of the network without projection but a learnable scalar scale. Our proposed framework reveals noise injection in StyleGAN as fuzzy reparameterization in Euclidean spaces, and extend it into generic manifolds (section 4.3).

3 The intrinsic drawbacks of traditional GANs

3.1 Optimal transportation and discontinuous generator.

Traditional GANs with Wasserstein distance is equivalent to the optimal transportation problem, where the optimal generator is the optimal transportation map. However, there is very rare chance for the optimal transportation map to be continuous, unless the support of Brenier potential is convex Caffarelli (1992). Considering that the Brenier potential of Wasserstein GAN is determined by the real data distribution and the inverse map of the generator, it is highly unlikely that the support of it is convex. This means that the optimal generator will be discontinuous, which is a fatal limitation to the capacity of GANs. Based on that, the authors further point out that, traditional GANs will hardly converge or converge to one continuous branch of the target mapping, leading to mode collapse Lei *et al.* (2019b). They then propose to find the continuous Brenier potential instead of the discontinuous transportation map. While in next paragraph, we show that this solution may not totally overcome the problem that traditional GANs encounter, given the structural limitations of neural networks. We refer the readers to Lei *et al.* (2019b); Caffarelli (1992) for more detailed demonstration.

3.2 Adversarial dimension trap.

Besides the above discontinuity problem, another drawback is the relatively low dimension of latent spaces compared with the high variance of the details in real world data. Picking images of human faces as an example, the hair, freckles, and wrinkles have extremely high degree of freedoms, which make traditional GANs often fail to capture them. The reiterative application of non-invertible CNN blocks make the situation even worse. Non-invertible CNN, which is a singular linear transformation, will drop the intrinsic dimensions of feature manifolds as information passed Strang *et al.* (1993). So during the feedforward procedure of the generator, dimensions of the feature spaces will keep dropping. Then, it will have a high chance that the valid dimension of the input latent space is lower than that of the real data. The relatively lower dimension of the input latent space will then, force the dimension of the support of the distribution of generated images lower than that of the real data, as no smooth mappings could increase the dimension. However, the discriminator, which measures the distance of these two distributions, will keep encouraging the generator to increase the dimension up to the same as the true data's. This contradictory functionality, as we show in the theorem below, induces severe punishment on the smoothness and invertibility of the generative model, which we refer as the adversarial dimension trap.

Theorem 1. ¹ For a deterministic GAN model and generator $G : \mathcal{Z} \rightarrow \mathcal{X}$, if the dimension of \mathcal{Z} is lower than \mathcal{X} 's, then at least one of the two cases must stand:

1. the generator cannot be Lipschitz;
2. the generator fails to capture the data distribution and is unable to do inversion.

Notice that this theorem implies much worse situation than it stated. As for any open sphere B in the data manifold \mathcal{X} , the generator restricted in the preimage of B also follow this theorem, which suggests bad properties of nearly every local neighbors.

The first issue can be addressed by not learning the generator directly by continuous neural network components, which suffices our proposed method in the next section. We will show how our method addresses the second issue.

4 Fuzzy reparameterization

The generator G in the traditional GAN is a composite of a series non-linear feature mappings, which can be denoted as $G(z) = f^k \circ f^{k-1} \circ \dots \circ f^1(z)$, where $z \sim \mathcal{N}(0, 1)$ is the standard Gaussian. Each feature mapping, which is typically a single layer CNN plus non-linear activations, carries out a certain purpose such as extracting multi-scale patterns, upsampling, or merging multi-head information. The whole network is then a deterministic mapping from the latent space \mathcal{Z} to the image space \mathcal{X} . While we propose to replace $f^i(x)$, $1 \leq i \leq k$ with

$$g^i(x) = \mu^i(x) + \sigma^i(x)\epsilon, \epsilon \sim \mathcal{N}(0, 1), x \in g^{i-1} \circ \dots \circ g^1(\mathcal{Z}). \quad (1)$$

¹As the common practice in the manifold learning community, our theorems and discussions are based on the Riemann manifold. Proofs to all the theorems are included in the supplementary material.

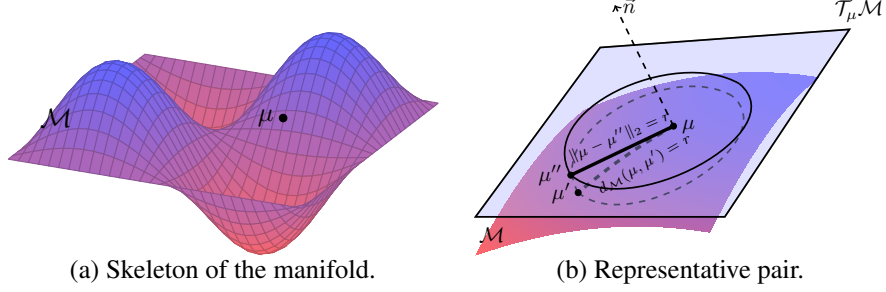


Figure 2: Illustration of the skeleton set and representative pair. The blue curve in (a) is the skeleton. In (b), the dashed sphere in \mathcal{M} is the geodesic ball, while the solid sphere in $\mathcal{T}_\mu \mathcal{M}$ is its projection onto the tangent space. The norm vector \vec{n} determines the final affine transformation into the Euclidean space.

We call it as a fuzzy reparameterization (FR) as it in fact learns a fuzzy equivalence relation of the original features, and use reparameterization to model the high dimensional feature manifolds. We believe that this is the proper form of generalization of noise injections in GANs, and will show the reasons and benefits in the following subsections.

It is not hard to see that our proposed method can be viewed as the extension of the reparameterization trick in VAEs Kingma & Welling (2013). While the reparameterization trick in VAEs serves to a differentiable solution to random variables and is only applied in the latent space, our method is a type of *deep* noise injection on feature maps of each layer to fix the defects in GAN architectures. Therefore, the purposes of using reparameterization in these two scenarios are different, thus leading to different theories that are presented in the next subsection.

4.1 Handling adversarial dimension trap through noise injection

As Sard’s theorem tells us Petersen *et al.* (2006), the key to solve the adversarial dimension trap is to avoid mapping low-dimensional feature spaces into high-dimensional ones, which looks like a pyramid structure. However, we really need the pyramid structure of the generator because the final output dimension of generated images is far more larger than that of the input latents. So the solution could be that, instead of mapping into the full feature spaces, we choose to map only onto the skeleton of the feature spaces and use random noises to fill up the remained space. For a compact manifold, it is easy to find that the intrinsic dimension of the skeleton set can be arbitrarily low by applying Heine–Borel theorem to the skeleton Rudin *et al.* (1964). By this way, the model can escape from the adversarial dimension trap.

Now we develop the idea in detail. The whole idea is based on approximating the manifold by the tangent polyhedron. Assume that the feature space \mathcal{M} is Riemann manifold embedded in \mathbf{R}^m . Then for any point $\mu \in \mathcal{M}$, the local geometry induces a coordinate transformation from a small neighbour of μ in \mathcal{M} to its projection onto the tangent space $\mathcal{T}_\mu \mathcal{M}$ at μ by the following theorem.

Theorem 2. *Given Riemann manifold \mathcal{M} embedded in \mathbf{R}^m , for any point $\mu \in \mathcal{M}$ let $\mathcal{T}_\mu \mathcal{M}$ be the tangent space at μ , then the exponential map Exp_μ induces a smooth diffeomorphism from a Euclidean ball $B_{\mathcal{T}_\mu \mathcal{M}}(0, r)$ centered at O to a geodesic ball $B_{\mathcal{M}}(\mu, r)$ centered at μ in \mathcal{M} . Thus $\{\text{Exp}_\mu^{-1}, B_{\mathcal{M}}(\mu, r), B_{\mathcal{T}_\mu \mathcal{M}}(0, r)\}$ form a local coordinate system of \mathcal{M} in $B_{\mathcal{M}}(\mu, r)$, which we call the normal coordinates. Thus we have:*

$$B_{\mathcal{M}}(\mu, r) = \text{Exp}_\mu(B_{\mathcal{T}_\mu \mathcal{M}}(0, r)) = \{\tau : \tau = \text{Exp}_\mu(v), v \in B_{\mathcal{T}_\mu \mathcal{M}}(0, r)\}. \quad (2)$$

Theorem 3. *The differential of Exp_μ at the origin of $\mathcal{T}_\mu \mathcal{M}$ is Identity. Thus Exp_μ can be approximated by*

$$\text{Exp}_\mu(v) = \mu + Iv + o(\|v\|_2). \quad (3)$$

Thus, if r in equation (2) is small enough, we can approximate $B_{\mathcal{M}}(\mu, r)$ by:

$$B_{\mathcal{M}}(\mu, r) \approx \mu + IB_{\mathcal{T}_\mu \mathcal{M}}(0, r) = \{\tau : \tau = \mu + Iv, v \in B_{\mathcal{T}_\mu \mathcal{M}}(0, r)\}. \quad (4)$$

Considering that $\mathcal{T}_\mu \mathcal{M}$ is an affine subspace of \mathbf{R}^m , the coordinates on $B_{\mathcal{T}_\mu \mathcal{M}}(0, r)$ admit an affine transformation into the coordinates on \mathbf{R}^m . Thus equation (4) can be written as:

$$B_{\mathcal{M}}(\mu, r) \approx \mu + IB_{\mathcal{T}_\mu \mathcal{M}}(0, r) = \{\tau : \tau = \mu + rT(\mu)\epsilon, \epsilon \in B(0, 1)\}. \quad (5)$$

We remind the readers that the linear component matrix $T(\mu)$ differs at different $\mu \in \mathcal{M}$ and is decided by the local geometrics near μ

In this formula, μ defines the center point and $rT(\mu)$ defines the shape of the approximated neighbour. So we call them a representative pair of $B_{\mathcal{M}}(\mu, r)$. Picking up a series of such representative pairs, which we refer as the skeleton set, we can construct a tangent polyhedron \mathcal{H} of \mathcal{M} . Thus instead of trying to learn feature manifold directly, we adopt a two-stage procedure. We first learn a map $f : x \mapsto [\mu(x), \sigma(x)]$ ($\sigma(x) \equiv rT(\mu(x))$) onto the skeleton set, then we use noise injection $g : x \mapsto \mu(x) + \sigma(x)\epsilon, \epsilon \sim \mathcal{U}(0, 1)$ (uniform distribution) to fill up the flesh of the feature space as shown in Figure 2.

However, the real world data often include fuzzy semantics. Even spatially-remote features could share some relations in common. It might be unwise to model it with unsmooth architectures such as local bounded sphere and uniform distribution. Thus we borrow the idea from fuzzy topology Ling & Bo (2003); Zhang & Zhang (2005); Murali (1989); Recasens (2010) which is designed to address this issue. It is well known that for any distance metrics $d(\cdot, \cdot)$, $e^{-d(\mu, \cdot)}$ admits a fuzzy equivalence relation for points near μ , which is similar with the density of Gaussian. The fuzzy equivalence relation could be viewed as a suitable smooth alternative to the sphere neighbor $B_{\mathcal{M}}(\mu, r)$. Thus we replace the uniform distribution with unclipped Gaussian². Under this settings, the first stage mapping in fact learns a fuzzy equivalence relation, while the second stage is a reparameterization technique. Notice that the skeleton set can have arbitrarily low dimension by Heine–Borel theorem. So the first-stage map can be smooth and well conditioned. For the second stage, we can show that it possess a smooth property in expectation by the following theorem.

Theorem 4. *Given $f : x \mapsto [\mu(x), \sigma(x)]^T$, f is locally Lipschitz and $\|\sigma\|_{\infty} = o(1)$. Define $g(x) \equiv \mu(x) + \sigma(x)\epsilon, \epsilon \sim \mathcal{N}(0, 1)$ (standard Gaussian), then for any bounded set U , $\exists L > 0$, s.t. $\mathbb{E}[\|g(x) - g(y)\|_2] \leq L\|x - y\|_2 + o(1), \forall x, y \in U$. Namely, the principal component of g is locally Lipschitz in expectation. Specifically, if the definition domain of f is bounded, then the principal component of g is globally Lipschitz in expectation.*

4.2 Properties of noise injection

As we have discussed, traditional GANs face two challenges: the discontinuous optimal generator and the adversarial dimension trap. Both of the two challenges will lead to an unsmooth generator. And Theorem 1 also implies an unstable training procedure considering the gradient explosion that may occur on the generator. Besides, the dimension drop in GAN will cause it hard to fit high-variance details as information keeps compressed along channels in the generator. While we apply noise injections to the network, we can theoretically overcome such problems if the representative pairs are constructed properly to capture the local geometrics. In that case, our model do not need to fit the discontinuous optimal transportation map, nor the image manifold with higher dimension than the network architecture can hold. Thus the training procedure will not encourage unsmooth generator, and can process more stably. Also, the extra noise can fill the loss of information compression so as to capture high-variance details, which has been discussed and proved in StyleGAN Karras *et al.* (2019b). We will experimentally evaluate the performance of our method from these aspects in sections 5.

4.3 Choice of $\mu(x)$ and $\sigma(x)$

As $\mu(x)$ stands for a particular point in the feature space, we simply model it by the traditional deep CNN architectures. $\sigma(x)$ is designed to fit the local geometrics of $\mu(x)$. While we assume the feature space to be smooth manifold, the local geometrics should only admit minor differences from $\mu(x)$. Thus we believe that $\sigma(x)$ should be determined by the spatial and semantic information contained in $\mu(x)$. This vision then guide us into the following settings:

$$\mu = \text{DCNN}(x), \sigma = \text{PixSum}(\mu), \quad (6)$$

$$\sigma = \alpha(A * (\sigma - \text{mean}(\sigma)) / \max(|\sigma|) + b) + (1 - \alpha)\mathbf{I}, \alpha \in [0, 1], \quad (7)$$

$$\sigma = r\sigma / \|\sigma\|_2, r > 0, \mu = \sigma * \mu, o = \mu + \sigma * \epsilon, \epsilon \sim \mathcal{N}(0, 1), \quad (8)$$

where **PixSum** stands for pixel-wise sum, o is the output, and A, b, α, r are learnable parameters. There are alternative forms for μ and σ with respect to various GAN architectures. However, modeling

²A detailed analysis about why unclipped Gaussian should be applied based on fuzzy topology is offered in the supplementary material.

Table 1: Metrics for various generator architectures. For StyleGAN2-based models, PPL scores are measured in the intermediate latent spaces.

GAN arch	FFHQ				LSUN-Church			
	PPL (\downarrow)	FID (\downarrow)	IS (\uparrow)	Precision (\uparrow)	PPL (\downarrow)	FID (\downarrow)	IS (\uparrow)	Precision (\uparrow)
DCGAN	2.97	45.29	2.42	0.764	33.30	51.18	2.56	0.646
DCGAN + Additive noise	3.14	44.22	2.52	0.761	22.97	54.01	2.68	0.477
DCGAN + FR	2.83	40.06	2.53	0.767	22.53	46.31	2.56	0.582
Bald StyleGAN2	28.44	6.87	4.54	0.673	425.7	6.44	2.58	0.573
StyleGAN2-NoPathReg	19.69	6.38	4.57	0.670	322.0	5.88	2.62	0.567
StyleGAN2	16.20	7.29	4.62	0.682	123.6	6.80	2.51	0.589
StyleGAN2-NoPathReg + FR	16.02	7.14	4.61	0.666	178.9	5.75	2.56	0.567
StyleGAN2 + FR	13.05	7.31	4.58	0.681	119.5	6.86	2.49	0.600

μ by deep CNNs and deriving σ through the spatial and semantic information of μ is universal for GANs, as it suits our theorem.

StyleGAN2 is also equipped with noise injection. But different from our design, they adopt a simple solution as follows:

$$\mu = \text{DCNN}(x), o = \mu + r * \epsilon, \epsilon \sim \mathcal{N}(0, 1), \quad (9)$$

where r is a learnable *scalar* parameter. This can be viewed as a special case of our method, where $T(\mu)$ in (5) is set to identity. Under this settings, the local geometrics are assumed to be universal among the feature manifold, which suggests a globally Euclidean structure. While our theory support this simplification and specialization, our choice of $\mu(x)$ and $\sigma(x)$ can suit broader and more usual occasions, where the feature manifolds are non-Euclidean. We denote this fashion of noise injection as additive noise injection, and will extensively study its performance compared with our choice in the following section.

5 Experiment

We conduct experiments on FFHQ faces, LSUN objects, and CIFAR-10 multiple classes. The GAN models we use are the baseline DCGAN Radford *et al.* (2015) (originally with no noise injection) and the state-of-the-art StyleGAN2 Karras *et al.* (2019a) (originally with additive noise injection). For StyleGAN2, we use config-e in the original paper due to that config-e achieves the best performance of path perceptual length (PPL) score. We inherit all the other experimental settings from StyleGAN2.

Image synthesis. The PPL Zhang *et al.* (2018) has been proven an effective metric for the perceived image quality Karras *et al.* (2019a). Considering its similarity to the expectation of the Lipschitz constant of the generator, it also can be viewed as a quantification of the smoothness of the generator. The path length regularizer is proposed in StyleGAN2 to regularize the PPL score by explicitly regularizing the Jacobian of the generator with respect to the intermediate latent space. We first compare the noise injection methods with the bald StyleGAN2, which remove the additive noise injection and path length regularizer in StyleGAN2. Through all the cases we can find that all types of noise injection significantly improve the PPL scores. As it is shown in Table 1, our method, without path length regularizer, can achieve comparable performance against StyleGAN2 in FFHQ dataset, and the performance can be further improved if combined with path length regularizer. Considering the extra GPU memory consuming of path length regularizer in training procedure, we believe that our method offers a computation-friendly alternative to StyleGAN2 as we observe smaller GPU memory usage of our method throughout all the experiments. Another benefit is that, despite that we enlarge the parameter volume, our method accelerates the convergence to the optimal FID scores. Figure 4 reports the FID curve as the iteration evolves. By our theorem, this can be explained as our method offers an architecture that is more consistent to the intrinsic geometrics of the feature space. Thus it is easier for the networks to fit.

In the LSUN-Church dataset, we observe an obvious improvement in FID scores compared with StyleGAN2. We believe that, this is because the the LSUN-Church data are scene images and contain various semantics of multiple objects, which are hard to fit for the original StyleGAN2 that is more suitable for single object synthesis. So our FR architecture offers more degree of freedom to the generator to fit the true distribution of the dataset. In all cases, our method outperforms

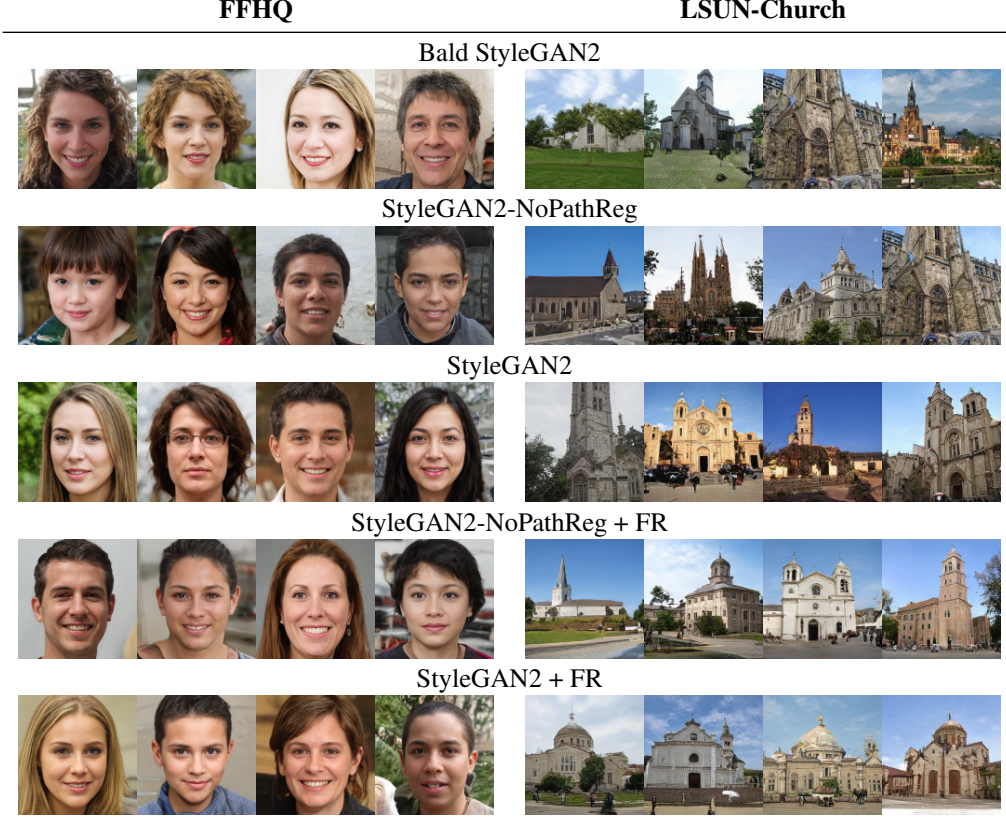


Figure 3: Synthesis images of different StyleGAN2-based models.

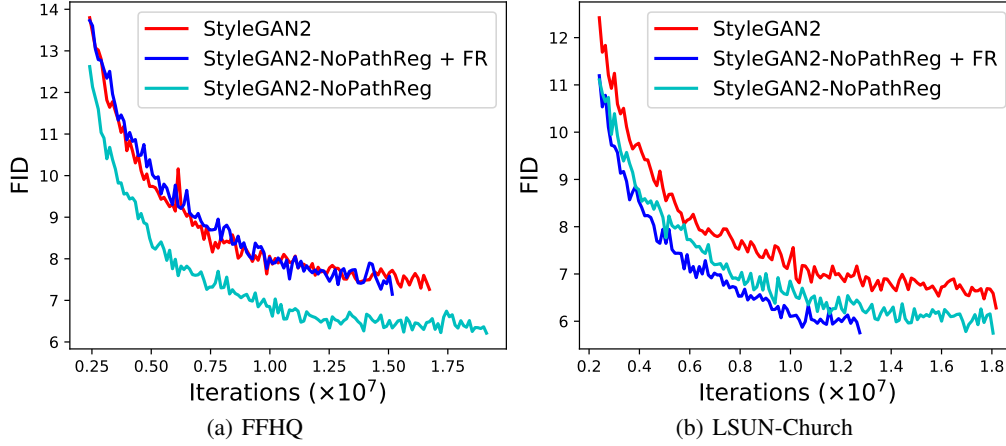


Figure 4: Comparison of FID curves. All curves are terminated by the optimal FID in 25M training iterations.

StyleGAN2-NoPathReg, which remove the path length regularizer in StyleGAN2, and is superior to StyleGAN2 in PPL scores if our method is combined with path length regularizer. This proves that our noise injection method is more proper than the one used in StyleGAN2. For DCGAN, as it does not possess the intermediate latent space, we cannot facilitate it with path length regularizer. So we only compare the additive noise injection with our FR method. Through all the cases we can find our method achieve the best performance in PPL and FID scores.

We also want to study whether our choice for $\mu(x)$ and $\sigma(x)$ can be applied to broader occasions. We further conduct experiments on a cat dataset, which consists of 100 thousand selected images from 800 thousand LSUN-Cat images by PageRank algorithm, to test whether our method could succeed

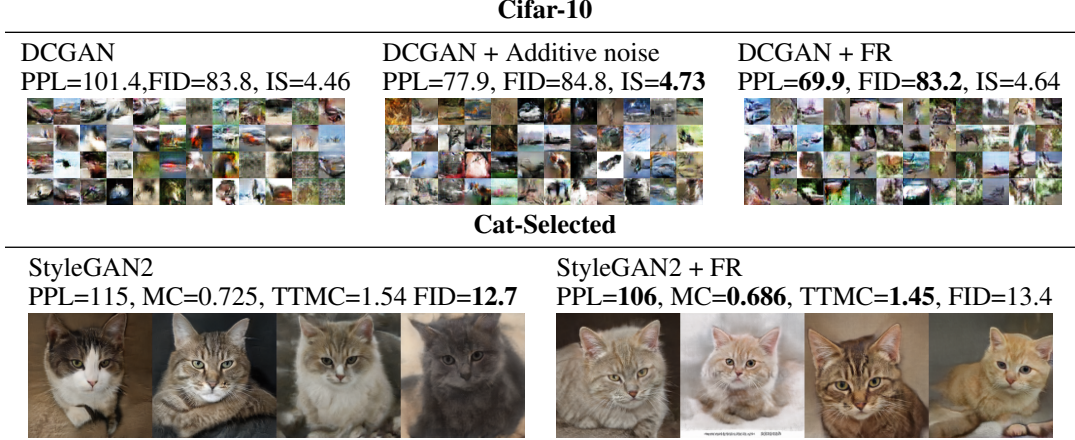


Figure 5: Image synthesis on CIFAR-10 and LSUN cats.

Table 2: Conditions for different GAN architectures. MC and TTMC (Top Thousand Mean Condition) are mean condition and mean value of the largest 1000 conditions at 50000 randomly sampled points in the input space respectively. The intermediate latent space is taken as the input space.

GAN arch	FFHQ		LSUN-Church	
	MC (\downarrow)	TTMC (\downarrow)	MC (\downarrow)	TTMC (\downarrow)
Bald StyleGAN2	0.943	2.81	2.31	6.31
StyleGAN2-NoPathReg	0.871	2.69	2.17	6.33
StyleGAN2	0.666	1.27	0.883	1.75
StyleGAN2-NoPathReg + FR	0.766	2.39	1.71	4.74
StyleGAN2 + FR	0.530	1.05	0.773	1.51

with insufficient training images. For DCGAN, we conduct extra experiments on CIFAR-10, to test whether our method could succeed in multi-class image synthesis. The results are reported in Figure 5, where we could see our method still dominates the performance against the compared methods in PPL scores with comparable FIDs.

Numerical stability. As we have analyzed before, noise injection should be able to improve the numerical stability of GAN models. To evaluate it, we examine the condition number of different GAN architectures. The definition of the condition number of a given function f can be found at Horn & Johnson (2013). It measures how sensitive a function is to changes or errors in the input, and how many errors in the output results from an error in the input. Considering the numerical infeasibility of the sup operator in the definition of condition number for functions, we resort to the following alternatives. We sample a batch of 50000 pairs of $(Input, Perturbation)$, severally from the input distribution and $\mathcal{N}(0, 1e-4)$, and compute the corresponding condition numbers. We compute the mean value and the mean value of the largest 1000 values of these 50000 condition numbers as Mean Condition (MC) and Top Thousand Mean Condition (TTMC) correspondingly to evaluate the condition of GAN models. We report the results on Table 2, where we can find that noise injection significantly improves the condition of GAN models, and our propose method dominates the performance.

GAN inversion. StyleGAN2 makes use of an intermediate latent space that holds the promise of enabling some controlled image modifications. This character motivate us to study the image embedding capability of our method via GAN inversion algorithms Abdal *et al.* (2019) as it may help further leverage the potential of GAN models. During the experiments, we find that the StyleGAN2 model develops an appetite for full-face, non-blocking human face images. For this type of images, we observe comparable performances for all the GAN architectures. We believe that this is because those images are close to the ‘mean’ face of FFHQ dataset Karras *et al.* (2019b), thus are easy to learn for the StyleGAN-based models. For those in the opposite, side-face, or partly blocked face images, the capacity of different models differ significantly. Noise injection methods outperform the bald StyleGAN2 by a large margin, and our method achieves the best performance. The detailed implementation and results are reported in the supplementary material.

6 Conclusion

In this paper, we propose a theoretical framework to explain the effect of noise injection technique in GANs. We prove that the generator can easily become unsmooth, and noise injection is a useful tool against it. We also derive a more proper formulation for noise injection based on our theoretical framework. We conduct experiments on various datasets to confirm its validity. Despite of the superiority compared with the existing methods, however, it still unclear whether it is optimal and universal among different networks and datasets for the specific neural network implementation of our formulation. In future work, we will further investigate the detailed implementation of noise injection, and find out much more powerful way to model local geometrics of feature spaces.

Broader Impact

This work potentially improves the GAN capacity to model real world data, such as images, videos, and texts with finer and more robust performance. If used properly, it might promote the applications of GAN models in real world scenes and commercial usage, such as data augmentation, image and video editing, and more general image processing. While the learning capacity may also arouse the concerns about illegally usage on sensitive sources, such as private files or confidential documents, and push more pressure to the enhancement of the data security.

Appendices

A Proof to theorems

A.1 Theorem 1

Proof. Denote the dimensions of $G(\mathcal{Z})$ and \mathcal{X} as d_G and $d_{\mathcal{X}}$, respectively. There are two possible cases for G : d_G is lower than $d_{\mathcal{X}}$, or d_G is higher than or equal to $d_{\mathcal{X}}$.

For the first case, a direct consequence is that, for almost all points in \mathcal{X} , there are no pre-images under G . This means that for an arbitrary point $x \in \mathcal{X}$, the possibility of $G^{-1}(x) = \emptyset$ is 1, as $\{x \in \mathcal{X} : G^{-1}(x) \neq \emptyset\} \subset G(\mathcal{Z}) \cap \mathcal{X}$, which is a zero measure set in \mathcal{X} . That means that the generator is unable to do inversion. Another consequence is that, the generated distribution P_g can never get aligned with real data distribution P_r . Namely, the distance between P_r and P_g cannot be zero for whatever distance metric. For the KL divergence, the distance will even become infinity.

For the second case, where $d_G \geq d_{\mathcal{X}} > d_{\mathcal{Z}}$. We simply show that a Lipschitz continuous function cannot map zero measure set into positive measure set. Specifically, the image of low dimensional space of a Lipschitz continuous function has measure zero. Thus if $d_G \geq d_{\mathcal{X}}$, G cannot be Lipschitz.

Now we prove our claim.

Suppose $f : \mathbb{R}^n \rightarrow \mathbb{R}^m$, $n < m$, f is Lipschitz with Lipschitz constant L . We show that $f(\mathbb{R}^n)$ has measure zero in \mathbb{R}^m . As \mathbb{R}^n is a zero measure subset of \mathbb{R}^m , by the Kirschbraun theorem Deimling (2010), f has an extension, still denoted as f , to a Lipschitz function of the same Lipschitz constant on \mathbb{R}^m . Then the problem reduces to proving that f maps zero measure set to zero measure set. For every $\epsilon > 0$, we can find countable union of balls $\{B_k\}_k$ of radius r_k such that $\mathbb{R}^n \subset \cup_k B_k$ and $\sum_k m(B_k) < \epsilon$ in \mathbb{R}^m , where $m(\cdot)$ is the Lebesgue measure in \mathbb{R}^m . But $f(B_k)$ is contained in a ball with radius Lr_k . Thus we have $m(f(\mathbb{R}^n)) \leq L^m \sum_k m(B_k) < L^m \epsilon$, which means that it is a zero measure set in \mathbb{R}^m . For the mappings between manifolds, using the chart system can turn it into the cases we analyze above, which completes our proof. \square

We also want to remind the readers that, even if the generator suits one of the cases in Theorem 1, the other case can still occur. For example, G could succeed in capturing the distribution of certain parts of the real data, while fail in the other parts. Then for the pre-image of those successfully captured data, the generator will not have finite Lipschitz constant.

A.2 Theorems 2 & 3

Theorems 2 & 3 are classical conclusions in Riemannian manifold. We refer readers to section 5.5 of Petersen *et al.* (2006) for detailed proofs and illustration.

A.3 Theorem 4

Proof.

$$\mathbf{E}[\|g(x) - g(y)\|_2] \leq \|\mu(x) - \mu(y)\|_2 + \mathbf{E}[\|\sigma(x)\epsilon - \sigma(y)\delta\|_2] \quad (10)$$

$$\leq L_\mu \|x - y\|_2 + 2C \|\sigma\|_\infty \leq L_\mu \|x - y\|_2 + o(1), \quad (11)$$

where C is a constant related to the dimension of the image space of σ and L_μ is the Lipschitz constant of μ . \square

B Why Gaussian distribution should be applied

We first introduce the notion of fuzzy equivalence relations.

Definition 1. A *t-norm* is a function $T : [0, 1] \times [0, 1] \rightarrow [0, 1]$ which satisfies the following properties:

1. *Commutativity*: $T(a, b) = T(b, a)$.
2. *Monotonicity*: $T(a, b) \leq T(c, d)$, if $a \leq c$ and $b \leq d$.
3. *Associativity*: $T(a, T(b, c)) = T(T(a, b), c)$.
4. *The number 1 acts as identity element*: $T(a, 1) = a$.

Definition 2. Given a *t-norm* T , a *T-equivalence relation* on a set X is a fuzzy relation E on X and satisfies the following conditions:

1. $E(x, x) = 1, \forall x \in X$ (*Reflexivity*).
2. $E(x, y) = E(y, x), \forall x, y \in X$ (*Symmetry*).
3. $T(E(x, y), E(y, z)) \leq E(x, z) \forall x, y, z \in X$ (*T-transitivity*).

Then it is easy to check that $T(x, y) = xy$ is a *t-norm*, and $E(x, y) = e^{-d(x, y)}$ is a *T-equivalence* for any distance metric d on X , as

$$T(E(x, y), E(y, z)) = e^{-(d(x, y) + d(y, z))} \leq e^{-d(x, z)} = E(x, z).$$

Considering that we want to contain the fuzzy semantics of real world data in our local geometries of feature manifolds, a natural solution will be that, we sample points from the local neighbor of μ with different density on behalf of different strength of semantic relations with μ . Those who contain stronger semantic relations would have larger densities to be sampled. A good framework to model this process is the fuzzy equivalence relations we mentioned above, where the degrees of membership E is used as the sampling density. However, remember that our expansion of the exponential map Exp_μ carries an error term of $o(\|v\|_2)$. We certainly do not want the local error to be out of control, and we also wish to constrain the sampling locally. Thus we accelerate the decrease of density when points depart from the center μ , and constrain the integral of E to be identity, which turns E into the density of standard Gaussian.

C Datasets

FFHQ Flickr-Faces-HQ (FFHQ) Karras *et al.* (2019b) is a high-quality image dataset of human faces, originally created as a benchmark for generative adversarial networks (GANs). The dataset consists of 70,000 high-quality PNG images and contains considerable variations in terms of age, pose, expression, hair style, ethnicity and image backgrounds. It also has good coverage of accessories such as eyeglasses, sunglasses, hats, etc.

Table 3: GPU environments for all experiments in this work.

Experiment	Environment
StyleGAN2 based GAN model training	8 NVIDIA Tesla V100-SXM2-16GB GPUs (DGX-1 station)
DCGAN based GAN model training	4 TITAN Xp GPUs
Metrics measurement	8 GeForce GTX 1080Ti GPUs
GAN inversion	1 TITAN Xp GPU

LSUN-Church and Cat-Selected LSUN-Church is the church outdoor category of LSUN dataset Yu *et al.* (2015), which consists of 126 thousands church images of various styles. Cat-Selected are 100 thousands cat images selected by ranking algorithm Zhou *et al.* (2004) from the cat category.

CIFAR-10 The CIFAR-10 dataset Krizhevsky *et al.* (2009) consists of 60,000 images of size 32x32. There are all 10 classes and 6000 images per class. There are 50,000 training images and 10000 test images.

D Implementation details

D.1 Metrics

Mean Condition (MC) and Top Thousand Mean Condition (TTMC) The condition number of a given function f is defines as

$$Cond(f) = \lim_{\delta \rightarrow 0} \sup_{\|\Delta x\| \leq \delta} \frac{\|f(x) - f(x + \Delta x)\| / \|f(x)\|}{\|\Delta x\| / \|x\|}. \quad (12)$$

It measures how sensitive a function is to changes or errors in the input, and how many errors in the output results from an error in the input. A function with a low condition number is said to be well-conditioned, while a function with a high condition number is said to be ill-conditioned. Considering the numerical infeasibility of the sup operator in the definition of condition number for functions, we resort to the following alternatives. We sample a batch of 50000 pairs of $(x, \Delta x)$ from the input distribution and $\mathcal{N}(0, 1e-4)$, and compute the corresponding condition numbers. We compute the mean value and the mean value of the largest 1000 values of these 50000 condition numbers as Mean Condition (MC) and Top Thousand Mean Condition (TTMC) respectively to evaluate the condition of GAN models.

Other metrics For all the other metrics, we inherit the implementation and settings from the official StyleGAN2 code.

D.2 Models

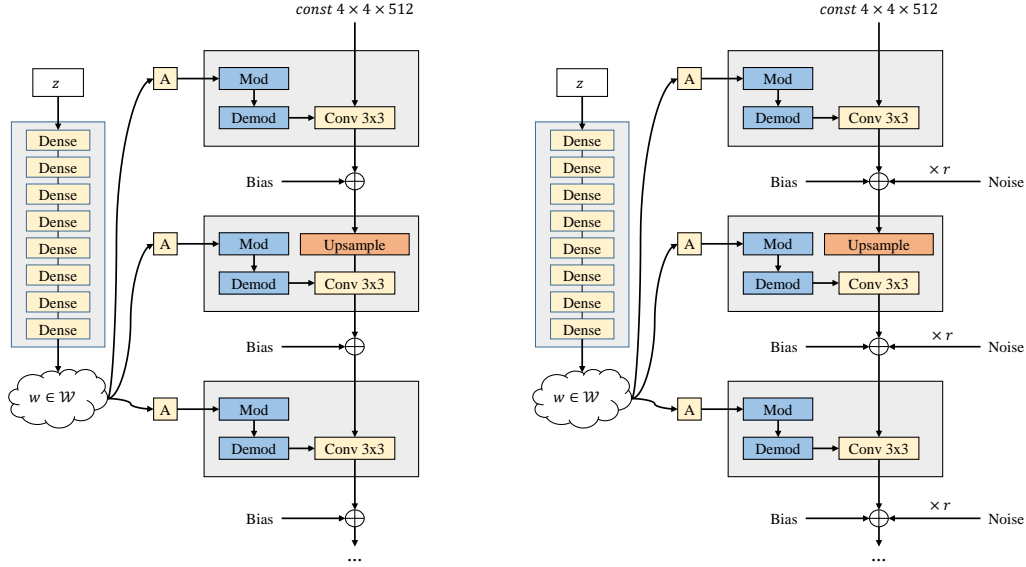
We illustrate the generator architectures of StyleGAN2 based methods in Figure 6. For all those models, the discriminators share the same architecture as the original StyleGAN2. The generator architecture of DCGAN based methods are illustrated in Figure 7. For all those models, the discriminators share the same architecture as the original DCGAN.

E Experiment environment

All experiments are carried out by TensorFlow 1.14 and Python 3.6 with CUDA Version 10.2 and NVIDIA-SMI 440.64.00. We basically build our code upon the framework of NVIDIA official StyleGAN2 code, which is available at <https://github.com/NVlabs/stylegan2>. We use a variety of servers to run the experiments as reported in Table 3.

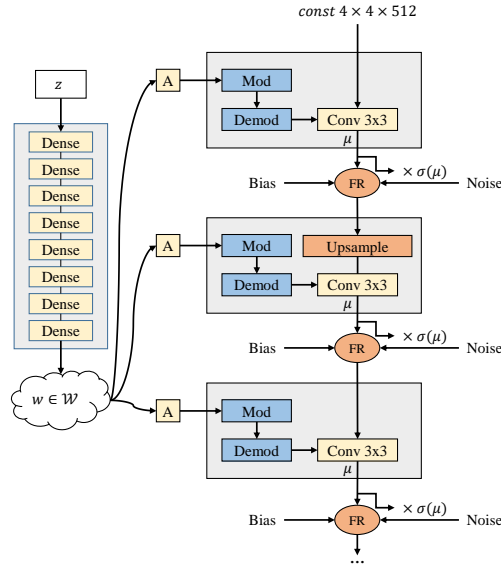
F Image encoding and GAN inversion

StyleGAN2 makes use of an intermediate latent space that holds the promise of enabling some controlled image modifications. This characteristic motivates us to study the image embedding



(a) Bald StyleGAN2.

(b) StyleGAN2.



(c) Fuzzy Reparameterization.

Figure 6: Generator architectures of StyleGAN2 based models. (a) The generator of Bald StyleGAN2. (b) The generator of StyleGAN2 and StyleGAN2-NoPathReg. (c) The generator of StyleGAN2 + FR and StyleGAN2-NoPathReg + FR. ‘Mod’ and ‘Demod’ denote the weight demodulation method proposed in section 2.2 of StyleGAN2 Karras *et al.* (2019a). A denotes a learned affine transformation from the intermediate latent space \mathcal{W} that produces a style.

capability of our method as it may help further leverage the potential of GAN models. Also, from a mathematical perspective, a well behaved generator should be easily invertible. In the last section, we have found that our method is well conditioned, which implies that it could be easily invertible. We adopt the methods in Image2StyleGAN Abdal *et al.* (2019) to perform GAN inversion and compare the mean square error and perceptual loss on a manually collected dataset of 20 images. The images are shown in Figure 8 and the quantitative results are provided in Table 4. For our FR methods, we further optimize the α parameter in Eq. 7 of section 4.3, which finetunes the local geometrics of the

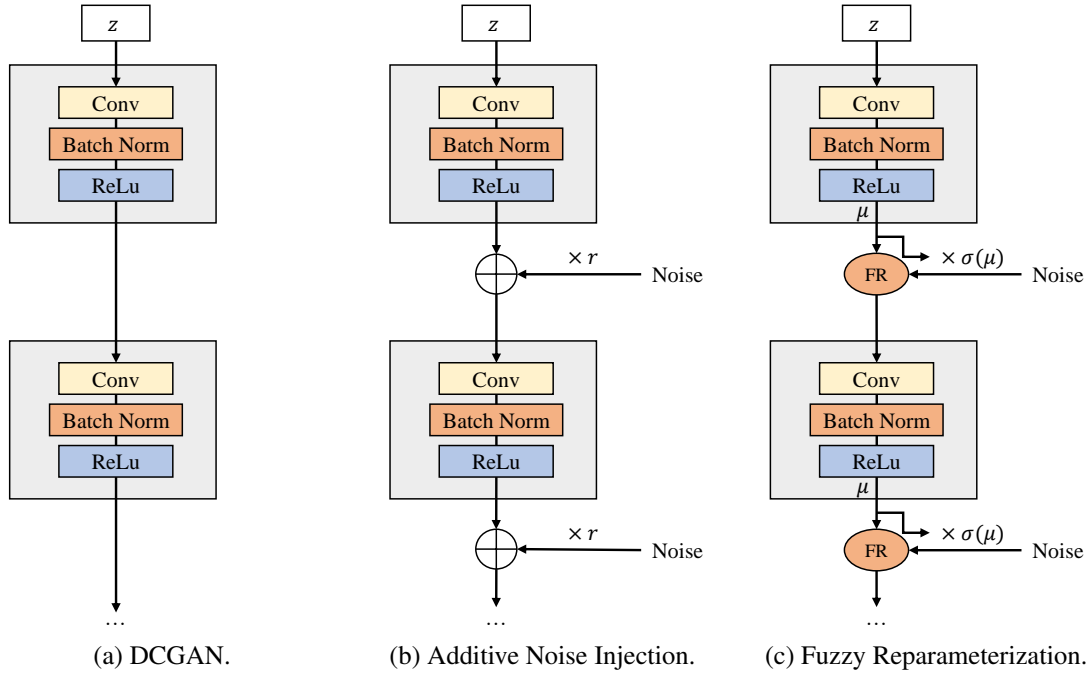


Figure 7: Generator architecture of DCGAN based models. (a) The generator of DCGAN. (b) The generator of DCGAN + Additive Noise. (c) The generator of DCGAN + FR.

Table 4: Image inversion metrics for different StyleGAN2 based models. The perceptual loss is the mean square distance of VGG16 features between the original and projected images as in Abdal *et al.* (2019)

GAN arch	Overall		Hard Cases	
	MSE (\downarrow)	Perceptual Loss (\downarrow)	MSE (\downarrow)	Perceptual Loss (\downarrow)
Bald StyleGAN2	1.34	5.42	2.86	11.34
StyleGAN2-NoPathReg	1.26	4.70	2.65	9.29
StyleGAN2	1.24	4.86	2.58	9.82
StyleGAN2-NoPathReg + FR	1.24	5.11	2.70	10.49
StyleGAN2 + FR	1.13	4.52	2.23	8.47

network to suit the new images that might not be settled in the model. Considering that α is limited to $[0, 1]$, we use $\frac{(\alpha^*)^t}{(\alpha^*)^t + (1 - \alpha^*)^t}$ to replace the original α and optimize t . The initial value of t is set to 1.0 and α^* is constant with the same value as α in the converged FR models.

During the experiments, we find that the StyleGAN2 model develops an appetite for full-face, non-blocking human face images. For this type of images (which we refer as regular case in Figure 9), we observe comparable performance for all the GAN architectures. We believe that this is because those images are closed to the ‘mean’ face of FFHQ dataset Karras *et al.* (2019b), thus easy to learn for the StyleGAN based models. For faces of large pose or partially blocked ones, the capacity of different models differs significantly. Noise injection methods outperform the bald StyleGAN2 by a large margin, and our method achieves the best performance.

References

Abdal, Rameen, Qin, Yipeng, & Wonka, Peter. 2019. Image2StyleGAN: How to Embed Images Into the StyleGAN Latent Space? *Pages 4432–4441 of: Proceedings of the IEEE International Conference on Computer Vision.*



Figure 8: Manually collected 20 images for GAN inversion.

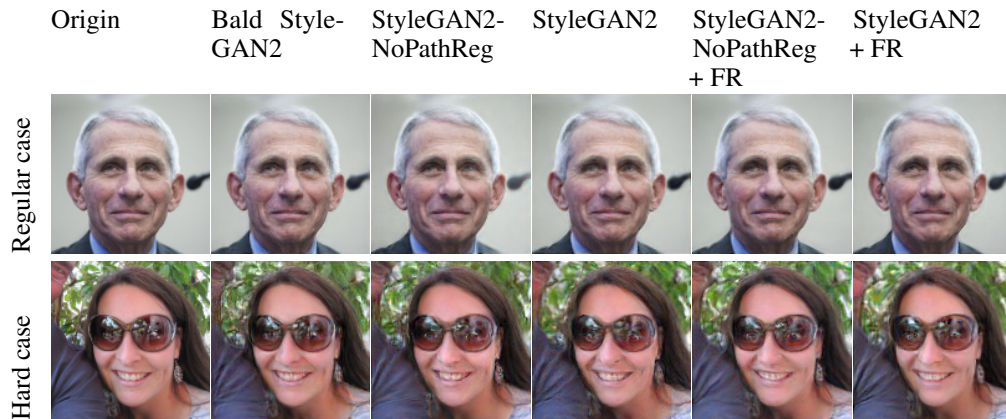


Figure 9: Projected Images to the intermediate latent space of StyleGAN2 based models.

Arjovsky, Martin, & Bottou, Léon. 2017. Towards Principled Methods for Training Generative Adversarial Networks. arXiv e-prints, art. *arXiv preprint arXiv:1701.04862*.

Arjovsky, Martin, Chintala, Soumith, & Bottou, Léon. 2017. Wasserstein GAN. *arXiv preprint arXiv:1701.07875*.

Baskin, Chaim, Liss, Natan, Chai, Yoav, Zheltonozhskii, Evgenii, Schwartz, Eli, Giryes, Raja, Mendelson, Avi, & Bronstein, Alexander M. 2018. Nice: Noise injection and clamping estimation for neural network quantization. *arXiv preprint arXiv:1810.00162*.

- Brock, Andrew, Donahue, Jeff, & Simonyan, Karen. 2018. *Large-Scale GAN Training for High Fidelity Natural Image Synthesis*.
- Bustos-Korts, Daniela, Malosetti, Marcos, Chapman, Scott, & van Eeuwijk, Fred. 2016. Modelling of genotype by environment interaction and prediction of complex traits across multiple environments as a synthesis of crop growth modelling, genetics and statistics. *Pages 55–82 of: Crop systems biology*. Springer.
- Caffarelli, Luis A. 1992. The regularity of mappings with a convex potential. *Journal of the American Mathematical Society*, **5**(1), 99–104.
- Deimling, Klaus. 2010. *Nonlinear functional analysis*. Courier Corporation.
- Denis, Jean-Baptiste, Piepho, Hans-Peter, & van Eeuwijk, Fred A. 1997. Modelling expectation and variance for genotype by environment data. *Heredity*, **79**(2), 162–171.
- Goodfellow, Ian J., Pouget-Abadie, Jean, Mirza, Mehdi, Xu, Bing, Warde-Farley, David, Ozair, Sherjil, Courville, Aaron, & Bengio, Yoshua. 2014. *Generative Adversarial Networks*.
- He, Zhezhi, Rakin, Adnan Siraj, & Fan, Deliang. 2019. Parametric noise injection: Trainable randomness to improve deep neural network robustness against adversarial attack. *Pages 588–597 of: Proceedings of the IEEE Conference on Computer Vision and Pattern Recognition*.
- Horn, Roger A., & Johnson, Charles R. 2013. *Matrix Analysis*. Cambridge University Press.
- Jenni, Simon, & Favaro, Paolo. 2019. On Stabilizing Generative Adversarial Training with Noise. *Pages 12145–12153 of: Proceedings of the IEEE Conference on Computer Vision and Pattern Recognition*.
- Karras, Tero, Laine, Samuli, Aittala, Miika, Hellsten, Janne, Lehtinen, Jaakko, & Aila, Timo. 2019a. Analyzing and improving the image quality of StyleGAN. *arXiv preprint arXiv:1912.04958*.
- Karras, Tero, Laine, Samuli, & Aila, Timo. 2019b. A style-based generator architecture for generative adversarial networks. *Pages 4401–4410 of: Proceedings of the IEEE Conference on Computer Vision and Pattern Recognition*.
- Kingma, Diederik P, & Welling, Max. 2013. Auto-encoding variational bayes. *arXiv preprint arXiv:1312.6114*.
- Krizhevsky, Alex, Hinton, Geoffrey, *et al.* 2009. Learning multiple layers of features from tiny images.
- Lei, Na, Su, Kehua, Cui, Li, Yau, Shing-Tung, & Gu, Xianfeng David. 2019a. A geometric view of optimal transportation and generative model. *Computer Aided Geometric Design*, **68**, 1–21.
- Lei, Na, Guo, Yang, An, Dongsheng, Qi, Xin, Luo, Zhongxuan, Yau, Shing-Tung, & Gu, Xianfeng. 2019b. Mode collapse and regularity of optimal transportation maps. *arXiv preprint arXiv:1902.02934*.
- Ling, Zhang, & Bo, Zhang. 2003. Theory of fuzzy quotient space (methods of fuzzy granular computing).
- Murali, V. 1989. Fuzzy equivalence relations. *Fuzzy sets and systems*, **30**(2), 155–163.
- Petersen, Peter, Axler, S, & Ribet, KA. 2006. *Riemannian geometry*. Vol. 171. Springer.
- Radford, Alec, Metz, Luke, & Chintala, Soumith. 2015. Unsupervised representation learning with deep convolutional generative adversarial networks. *arXiv preprint arXiv:1511.06434*.
- Recasens, Jordi. 2010. *Indistinguishability operators: Modelling fuzzy equalities and fuzzy equivalence relations*. Vol. 260. Springer Science & Business Media.
- Romagosa, I, & Fox, PN. 1993. Genotype \times environment interaction and adaptation. *Pages 373–390 of: Plant breeding*. Springer.

- Rudin, Walter, *et al.* 1964. *Principles of mathematical analysis*. Vol. 3. McGraw-hill New York.
- Srivastava, Nitish, Hinton, Geoffrey, Krizhevsky, Alex, Sutskever, Ilya, & Salakhutdinov, Ruslan. 2014. Dropout: a simple way to prevent neural networks from overfitting. *The journal of machine learning research*, **15**(1), 1929–1958.
- Strang, Gilbert, Strang, Gilbert, Strang, Gilbert, & Strang, Gilbert. 1993. *Introduction to linear algebra*. Vol. 3. Wellesley-Cambridge Press Wellesley, MA.
- van Eeuwijk, Fred A. 1996. *Between and beyond additivity and non-additivity: the statistical modelling of genotype by environment interaction in plant breeding*. Van Eeuwijk.
- Via, Sara, & Lande, Russell. 1985. Genotype-environment interaction and the evolution of phenotypic plasticity. *Evolution*, **39**(3), 505–522.
- Westcott, Brian. 1986. Some methods of analysing genotype—environment interaction. *Heredity*, **56**(2), 243–253.
- Yu, Fisher, Seff, Ari, Zhang, Yinda, Song, Shuran, Funkhouser, Thomas, & Xiao, Jianxiong. 2015. Lsun: Construction of a large-scale image dataset using deep learning with humans in the loop. *arXiv preprint arXiv:1506.03365*.
- Zhang, Ling, & Zhang, Bo. 2005. Fuzzy reasoning model under quotient space structure. *Information Sciences*, **173**(4), 353–364.
- Zhang, Richard, Isola, Phillip, Efros, Alexei A, Shechtman, Eli, & Wang, Oliver. 2018. The unreasonable effectiveness of deep features as a perceptual metric. *Pages 586–595 of: Proceedings of the IEEE Conference on Computer Vision and Pattern Recognition*.
- Zhou, Dengyong, Weston, Jason, Gretton, Arthur, Bousquet, Olivier, & Schölkopf, Bernhard. 2004. Ranking on data manifolds. *Pages 169–176 of: Advances in neural information processing systems*.